



Tailoring the glass forming ability, mechanical properties and corrosion resistance of Cu–Zr–Al bulk metallic glasses by yttrium addition

Mehdi Malekan^{a,*}, Reza Rashidi^b, Mansoor Bozorg^c, Nick Birbilis^d

^a School of Metallurgy and Materials Engineering, College of Engineering, University of Tehran, P.O. Box 11155-4563, Tehran, Iran

^b Applied Science and Technology Department, Politecnico di Torino, Corso Duca degli Abruzzi 24, Torino, 10129, Italy

^c Department of Materials Science and Engineering, Shahrood University of Technology, Shahrood, Iran

^d College of Engineering and Computer Science, Australian National University, Acton, ACT, 2601, Australia

ARTICLE INFO

Keywords:

Bulk metallic glass
Corrosion
Glass forming ability
Mechanical properties

ABSTRACT

The effect of yttrium (Y) on the glass-forming ability (GFA), mechanical properties and corrosion of $(\text{Cu}_{50}\text{Zr}_{43}\text{Al}_7)_{100-x}\text{Y}_x$ ($x = 0, 2$ and 4 , in at. %) alloys was investigated. The GFA of $\text{Cu}_{50}\text{Zr}_{43}\text{Al}_7$ alloy was improved by the addition of Y, with a GFA of 15 mm in diameter being obtained for $(\text{Cu}_{50}\text{Zr}_{43}\text{Al}_7)_{98}\text{Y}_2$. In uniaxial compression, the bulk metallic glasses (BMGs) exhibited a limited plastic strain of less than 1%, however compressive fracture strength and Young's modulus of 1787–2006 MPa and 101–122 GPa were achieved, respectively. Fracture surfaces and shear bands were studied via scanning electron microscopy. The corrosion behavior of BMGs was analyzed by potentiodynamic polarization experiments and electrochemical impedance spectroscopy (EIS) in acidic chloride (1 M HCl) and neutral chloride (0.6 M NaCl) environments. As a result of the Y addition, the corrosion resistance of the base BMG was improved.

1. Introduction

As structural materials, bulk metallic glasses (BMGs) present unique mechanical, physical and chemical properties [1–5]. Amongst the ‘glassy’ (non-crystalline) alloys that can be formed in bulk sizes – where bulk refers to dimensions of >1 mm – the range of copper (Cu) based BMGs with high glass-forming ability (GFA) are promising for industrial applications. The Cu-based BMGs possess a relatively high strength, high thermal stability and low cost [6–14]. A combination of high GFA, good mechanical properties and good corrosion resistance is expected from CuZr-based BMGs.

As with most engineering alloys, the corrosion resistance of CuZr-based BMGs is a function of microstructure and chemical homogeneity [15]. In other words, the presence of structural heterogeneities, including the presence of crystalline phases, in the glassy matrix will influence the corrosion of BMGs. A number of studies have been conducted on the corrosion behavior of CuZr-based BMGs in different environments. Among various CuZr-based BMGs, Cu–Zr–Al glassy alloys are promising candidate for structural applications due to their unique properties. Furthermore, it has been observed that the properties of glassy alloys may be improved by minor additions of specific alloying elements. There are different considerations for selecting alloying

elements, including the requirement to maintain or improve GFA, mechanical and physical properties, and corrosion resistance. Several CuZr-based BMGs have been developed in recent years in both thin and bulk forms. It has been reported that the GFA and mechanical properties of CuZr-based BMGs can be influenced by the addition of yttrium (Y) [10,16–19]. Xu et al. [20] reported that the fully amorphous $\text{Cu}_{46}\text{Zr}_{47-x}\text{Al}_7\text{Y}_x$ ($0 \leq x \leq 10$) BMGs with diameters from 4 mm to 1 cm could be prepared by injection mold casting. Hong et al. [16] observed that the addition of Y improved GFA while decreasing fracture strength, attributed to a decreased binding energy resulting from the addition of Y.

The corrosion properties of BMGs in response to the minor addition of alloying elements has not been widely explored in the context of CuZr-based BMGs. In one such study, Nie et al. [21] reported that micro-alloying a CuZr-based BMG with Ti was capable of improving corrosion resistance. However, the addition of Ti deteriorated the thermal stability of the BMG. The same effects were reported by Tam et al. [22] when exploring minor additions of Nb to a CuZr-based BMG. Zhang et al. [23] added 2–8 at. % of La to the binary $\text{Cu}_{50}\text{Zr}_{50}$ BMG, observing that La additions enhanced corrosion resistance by deterring the selective dissolution. Hua et al. [24] partially substituted Co with Ag in a Zr–Co–Al BMG; noting that the addition of Ag improved the corrosion

* Corresponding author.

E-mail address: mmalekan@ut.ac.ir (M. Malekan).

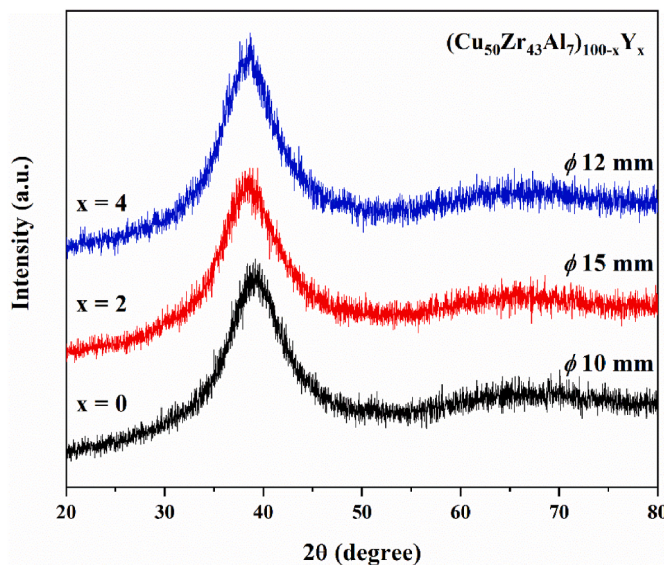


Fig. 1. XRD patterns of as-cast $(\text{Cu}_{50}\text{Zr}_{43}\text{Al}_7)_{100-x}\text{Y}_x$ ($x = 0, 2$ and 4 at. %) BMGs.

resistance by a mechanism they attributed to the increase of Zr concentration in the surface passive layer. The addition of Indium (In) was explored by Jinhong et al. [25] in two Cu–Zr–Ti alloy systems in which corrosion behavior was assessed in a NaCl solution. The authors revealed that both a minor and moderate addition of In to both of the Cu–Zr–Ti BMGs explored resulted in an improved corrosion resistance; however excessive In additions degraded corrosion resistance. Whilst some research has been carried out regarding the corrosion properties of BMGs containing rare earth element additions; there remains a need for further studies of the effect of rare earth elements on corrosion of BMGs. In the present study, the effects of alloyed yttrium (Y) on the glass-forming ability, mechanical properties and corrosion behavior of a Cu–Zr–Al BMG were explored.

2. Experimental procedures

Alloy ingots were prepared by arc melting the mixtures of pure Cu (99.99%), Zr (99.9%), Al (99.999%) and Y (99.99%) in a purified argon atmosphere. Cylindrical rods with diameters of 2–16 mm were prepared from the ingots by a cooled copper mold casting method. The glassy structure of as-cast rods was examined by X-ray diffraction (XRD), using Cu K α radiation. Mechanical properties in a compressive deformation mode were measured at least three times for each alloy using an Instron® instrument. The test specimen had a diameter of 2 mm and a length of 4 mm, with a strain rate of $5 \times 10^{-4} \text{ s}^{-1}$. To minimize the effect of friction on test results, specimen surfaces were polished in a parallel manner. The compressive test was applied whilst placing the samples between two alumina plates. The Young's modulus was also determined accurately via the utilization of a strain gauge attached to the lateral surface of the samples. Fracture surface were examined by scanning electron microscopy (SEM, HITACHI, S-4800).

Electrochemical testing employed a conventional three electrode cell, and an Iviumstat® potentiostat equipped with electrochemical impedance spectroscopy module. The counter electrode used was platinum and the reference electrode used was a saturated calomel electrode (SCE), separated from the cell by a glass frit. Electrochemical tests were performed in 0.6 M NaCl (as a seawater simulant) and 1 M HCl (strong acid) solutions. Electrochemical impedance spectroscopy (EIS) measurements were carried out at open circuit potential after a stabilized period and conducted using a sine wave with potential perturbation amplitude of 5 mV in the frequency range of 100 kHz to 10 MHz. All the reported potentials in this work were measured with respect to the SCE.

Table 1

Mechanical properties of the $(\text{Cu}_{50}\text{Zr}_{43}\text{Al}_7)_{100-x}\text{Y}_x$ ($x = 0, 2$ and 4 at. %) bulk glassy alloys.

Alloy	E (GPa)	σ_f (MPa)
$\text{Cu}_{50}\text{Zr}_{43}\text{Al}_7$	122 ± 2	2006 ± 5
$(\text{Cu}_{50}\text{Zr}_{43}\text{Al}_7)_{98}\text{Y}_2$	103 ± 2	1920 ± 15
$(\text{Cu}_{50}\text{Zr}_{43}\text{Al}_7)_{96}\text{Y}_4$	101 ± 1	1787 ± 7

Corrosion current density were estimated with using potentiodynamic polarization, polarization curves were obtained from -250 mV (vs. open circuit potential) to $+500$ mV with a sweep rate of 1 mV/s. Specimen surfaces were observed with Field Emission Scanning Electron Microscopy (FESEM, ZEISS Sigma 300- HV).

3. Results and discussion

3.1. Glass forming ability

Fig. 1 reveals the XRD patterns of the as-cast $(\text{Cu}_{50}\text{Zr}_{43}\text{Al}_7)_{100-x}\text{Y}_x$ alloy rods with different diameters.

It was determined that the XRD patterns consist of only broad diffraction maxima without any detectable (sharp) Bragg peaks, indicating the rods have a glassy structure. The $\text{Cu}_{50}\text{Zr}_{43}\text{Al}_7$ alloy has a GFA of 10 mm. Adding Y improved glass formation. In this regard, $(\text{Cu}_{50}\text{Zr}_{43}\text{Al}_7)_{98}\text{Y}_2$ alloy exhibits the highest GFA of 15 mm in diameter among $(\text{Cu}_{50}\text{Zr}_{43}\text{Al}_7)_{100-x}\text{Y}_x$ alloys tested. With the further addition of Y to 4 at. %, the GFA of $(\text{Cu}_{50}\text{Zr}_{43}\text{Al}_7)_{96}\text{Y}_4$ alloy decreased to 12 mm – which remains higher than the base (Y free) alloy. Accordingly, it can be suggested that a suitable addition of Y may effectively suppress the precipitation of crystalline phases, and hence further facilitate the glass formation during solidification of the alloys. In our previous study [26], the role of the optimum yttrium content in improving the GFA was scrutinized considering atomic, topological, and thermodynamics concepts. It was also posited that the main mechanism through which Y may enhance GFA is by permitting a more densely packed atomic structure, as well as by scavenging oxygen - an undesirable element in glass production systems due to the relative reactivity of Y compared to Cu, Zr and Al.

The mechanism by which the addition of rare earth elements (REs) to a CuZr metallic glass improves its glass-forming ability (GFA) is still an area of active research. There are different proposed mechanisms for the improved GFA, based on computational methods [27], topological theories [28], and empirical rules [1]. Additionally, the proper addition of Y at approximately 2% can significantly improve the GFA of CuZr BMGs by scavenging oxygen, hindering diffusion, and suppressing the growth of eutectic clusters and the precipitation of primary dendrite phases [26,29,30].

3.2. Mechanical properties

The compressive fracture strength and Young's modulus of the $(\text{Cu}_{50}\text{Zr}_{43}\text{Al}_7)_{100-x}\text{Y}_x$ alloys are summarized in **Table 1**.

The $(\text{Cu}_{50}\text{Zr}_{43}\text{Al}_7)_{100-x}\text{Y}_x$ ($x = 0, 2$ and 4 at. %) BMGs revealed good mechanical properties, i.e., compressive fracture strength (σ_f) of 1787–2006 MPa and Young's modulus (E) of 101–122 GPa. The highest fracture strength and Young's modulus of 2006 MPa and 122 GPa were obtained for the $\text{Cu}_{50}\text{Zr}_{43}\text{Al}_7$ alloy (i.e., the Y-free alloys). It was observed that the fracture strength and Young's modulus both decreased with the addition of Y. One hypothesis is that the addition of the comparatively large Y atom (where Y has a larger atomic radius) may weaken inter-atomic bonding and lead to a lower fracture strength and Young's modulus.

Wang et al. [31] have observed that the minor addition of Y stimulates the formation of icosahedral clusters in the matrix while still maintaining the system's amorphous nature. Accordingly, these

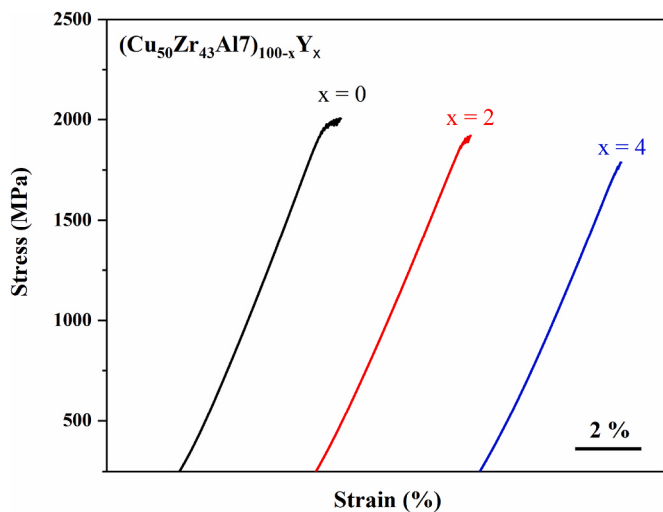


Fig. 2. Compressive stress-strain curves of as-cast $(\text{Cu}_{50}\text{Zr}_{43}\text{Al}_7)_{100-x}\text{Y}_x$ BMGs.

icosahedral structures effectively increase the viscosity of the super-cooled liquid and consequently raise the energy barrier for crystallization. On the other hand, Lee et al. [32] have proposed that, in addition to the population of the icosahedral clusters, the interpenetrating connection (connectivity) of icosahedral clusters plays a critical role in both the local and bulk mechanical properties of Cu–Zr MGs. Therefore, one possible explanation for the role of Y in the GFA and mechanical properties of the base BMG of our study is that Y could stimulate a more tightly packed atomic structure, including icosahedral clusters, which is favorable for glass forming and avoiding short-range order. However, the quantity and organization of these clusters may not be sufficient to improve the mechanical strength.

The nominal compressive stress-strain curves of the $(\text{Cu}_{50}\text{Zr}_{43}\text{Al}_7)_{100-x}\text{Y}_x$ BMGs are presented in Fig. 2.

It was confirmed via scanning electron microscopy that the deformation and final fracture of all alloys occurred along the maximum shear stress plane at an angle of 45° to the direction of applied load (Fig. 3a). In addition, the well-developed vein-like patterns were observed on the fracture surface of the $(\text{Cu}_{50}\text{Zr}_{43}\text{Al}_7)_{100-x}\text{Y}_x$ samples (Fig. 3b), which originates from shear deformation of the glassy matrix. The $(\text{Cu}_{50}\text{Zr}_{43}\text{Al}_7)_{100-x}\text{Y}_x$ ($x = 0, 2$ and 4 at. %) BMGs exhibit a limited plastic strain of less than 1% . This suggests that the plastic deformation is highly localized into a single or few shear bands, which initiate and rapidly propagate across the samples at an angle of approximately 45° to the loading axis. A shear band can also initiate a crack which will cause macroscopic fracture.

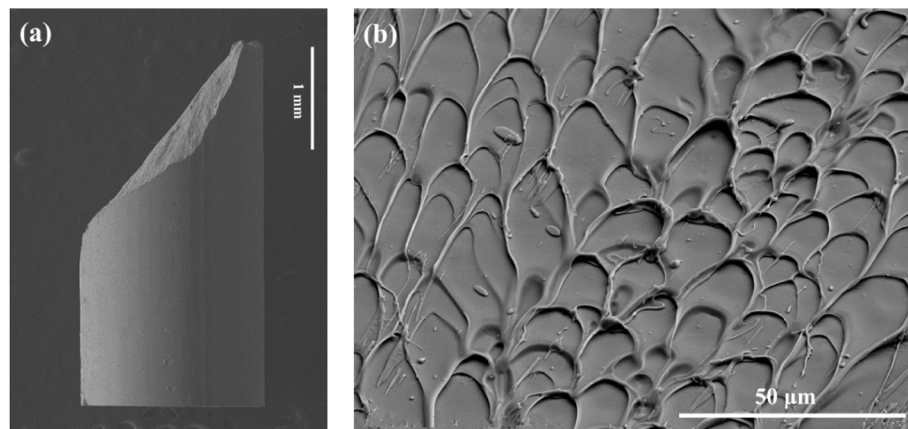


Fig. 3. Scanning electron micrographs revealing (a) lateral (b) fracture surface appearance of $(\text{Cu}_{50}\text{Zr}_{43}\text{Al}_7)_{98}\text{Y}_2$ BMG rod with a diameter of 2.0 mm .

3.3. Electrochemical response

Electrochemical impedance spectroscopy (EIS) was performed on the different BMG samples and pure copper as a reference in both 0.6 M NaCl and 1 M HCl solutions. The Nyquist plots obtained from EIS tests are shown in Fig. 4.

As is well reported in the literature [33–36], the Nyquist plot of copper sample in both HCl and NaCl solutions consists of a capacitance loop at high to intermediate frequencies, whilst presents a characteristic Warburg response at lower frequencies – indicating that electrochemical reactions upon the Cu surface are under diffusion (mass transport) control. The scale of the Nyquist curves is unique for each of the BMG samples, revealing a higher overall impedance relative to pure Cu, also concomitant with the absence of the Warburg response (diffusion control). With the addition of Y to the BMGs, the general shape of Nyquist curves was not changed; suggesting that the corrosion mechanism did not significantly alter with the addition of alloyed Y – however the resistance to charge transfer increased with Y.

Regarding the electrochemical performance of the BMGs tested, in both test environments the Nyquist curves at high frequencies consisted of a compressed capacitive loop. This capacitive loop is related to the double layer capacitance and charge transfer resistance. At low frequencies there is an inductive loop in the Nyquist curve – for all the BMGs tested, and in both electrolytes utilized. The presence of an inductive loop is attributed to the manifestation of a time dependent evolution in the relationship between the applied potential and resultant current response – indicative of surface reactivity. Such reactivity is not strictly (and solely) a dissolution process, but may also represent a surface filming process. For example, Singh et al. [37] ascribed the presence of an inductive loop in the Nyquist plot of steel in a sweet corrosion environment to the desorption of corrosion products. Other researchers have attributed the existence of a low frequency inductive loop to the adsorption of Cl^- ions to the surface [38,39]. Formation or adsorption of corrosion products on the surface during dissolution has also been reported as a reason for the presences of inductive loop [40, 41]. However, the presence of an inductive loop is suggestive that a corrosion or dissolution process is occurring in the timescale probed by low frequency impedance measurements.

For the Nyquist plots herein including the presence of a low frequency inductive loop, the point of intersection between the capacitive loop and the real axis represents the sum of the solution resistance and the charge transfer resistance [42–44]. Accordingly, Fig. 5 reports the determined values of charge transfer resistance for specimens tested in 1 M HCl and 0.6 M NaCl solutions. As shown in Fig. 5, copper specimens revealed the lowest value of charge transfer resistance (R_{ct}) in both solutions, and hence the lowest resistance to corrosion among the samples tested. It was noted that increasing Y content in BMGs resulted in an

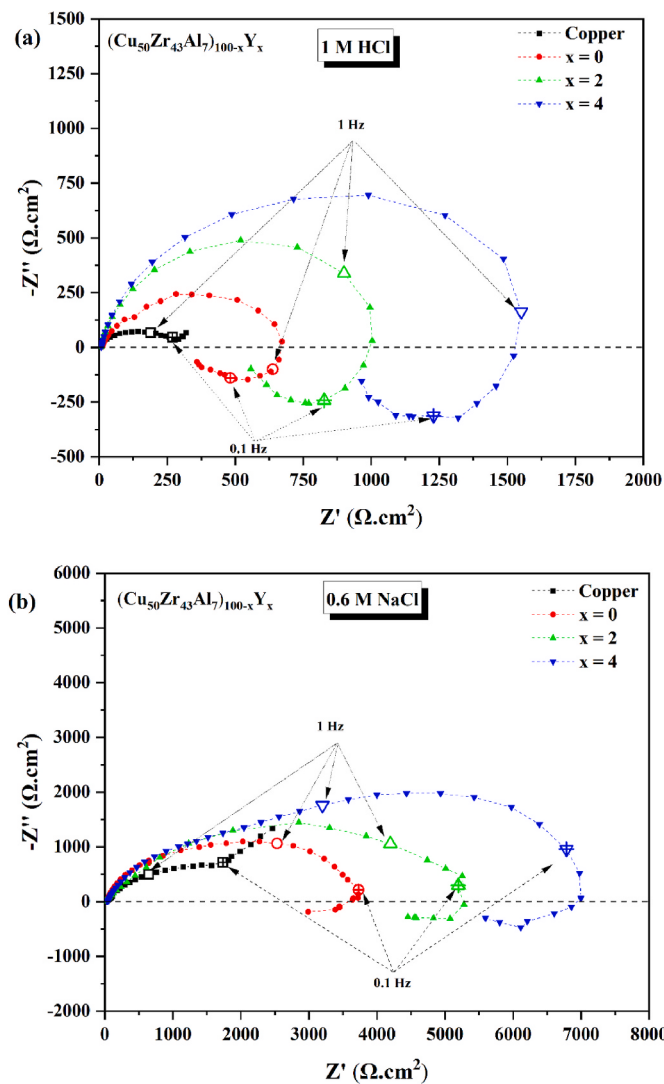


Fig. 4. Nyquist diagram of copper and $(\text{Cu}_{50}\text{Zr}_{43}\text{Al}_7)_{100-x}\text{Y}_x$ samples in a) 1 M HCl, and b) 0.6 M NaCl solutions.

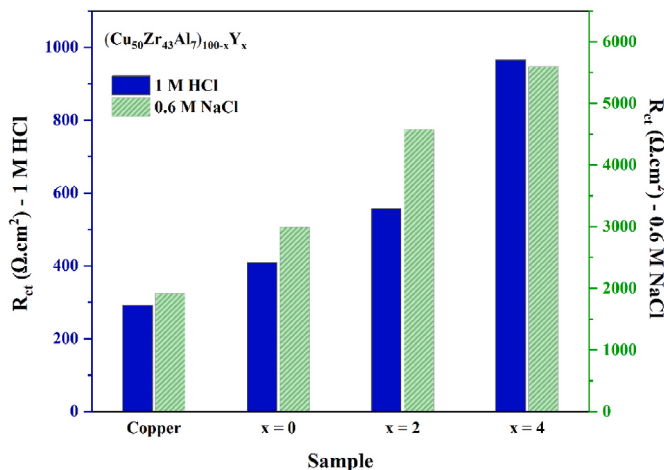


Fig. 5. Charge transfer resistance of copper and $(\text{Cu}_{50}\text{Zr}_{43}\text{Al}_7)_{100-x}\text{Y}_x$ samples in 1 M HCl and 0.6 M NaCl solutions.

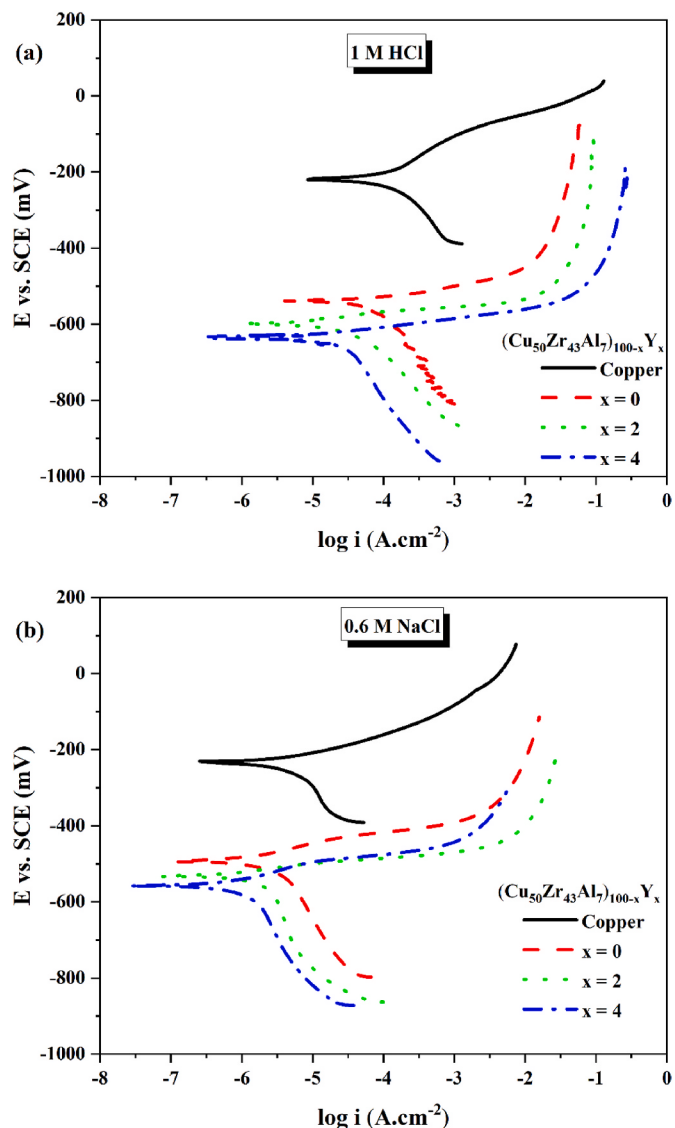


Fig. 6. Polarization curves of copper and $(\text{Cu}_{50}\text{Zr}_{43}\text{Al}_7)_{100-x}\text{Y}_x$ samples in a) 1 M HCl, and b) 0.6 M NaCl solutions.

increase in the charge transfer resistance. The $(\text{Cu}_{50}\text{Zr}_{43}\text{Al}_7)_{98}\text{Y}_4$ BMG indicated the highest charge transfer resistance.

In order to more holistically investigate on the corrosion behavior of the alloys studied herein, polarization testing was also performed in the two environments. The results of the potentiodynamic electrochemical polarization testing are shown in Fig. 6.

Similar potentiodynamic polarization curves to those in Fig. 6 have been reported for copper-based amorphous alloys in acidic and chloride solutions [45–47]. A feature of the polarization curves of BMG samples tested herein, appears to be that the curves (over a range of potentials) ‘shifted to the left’ relative to the pure copper sample, in addition to a notably lower corrosion potential (E_{corr}) relative to pure copper. Upon anodic polarization, a rise in the anodic current density with increasing potential above E_{corr} was observed, indicating anodic dissolution of the BMG samples in both 0.6 M NaCl and 1 M HCl solutions [45]. From inspection of Fig. 6 (a) and 6 (b), the addition of Y has a negligible impact on the slopes of the polarization curves. The results of the analysis of electrochemical polarization curves are presented in Table 2.

As noted by the results in Table 2, the addition of Y influenced the corrosion rate as measured by potentiodynamic polarization, in both testing environments. In 1 M HCl solution, the BMG samples revealed a

Table 2

Open circuit potential (E_{OCP}), corrosion potential (E_{corr}), and corrosion current density (i_{corr}), for copper and $(\text{Cu}_{50}\text{Zr}_{43}\text{Al}_7)_{100-x}\text{Y}_x$ samples determined in various electrolyte solutions by potentiodynamic polarization.

Sample	0.6 M NaCl			1 M HCl		
	E_{OCP} (mV _{SCE})	E_{corr} (mV _{SCE})	i_{corr} ($\mu\text{A}/\text{cm}^2$)	E_{OCP} (mV _{SCE})	E_{corr} (mV _{SCE})	i_{corr} ($\mu\text{A}/\text{cm}^2$)
Copper	-141	-235	12	-138	-222	165
$\text{Cu}_{50}\text{Zr}_{43}\text{Al}_7$	-547	-489	4.4	-560	-540	120.5
$(\text{Cu}_{50}\text{Zr}_{43}\text{Al}_7)_{98}\text{Y}_2$	-613	-533	3.1	-615	-590	53.8
$(\text{Cu}_{50}\text{Zr}_{43}\text{Al}_7)_{96}\text{Y}_4$	-621	-556	1.5	-709	-628	38.0

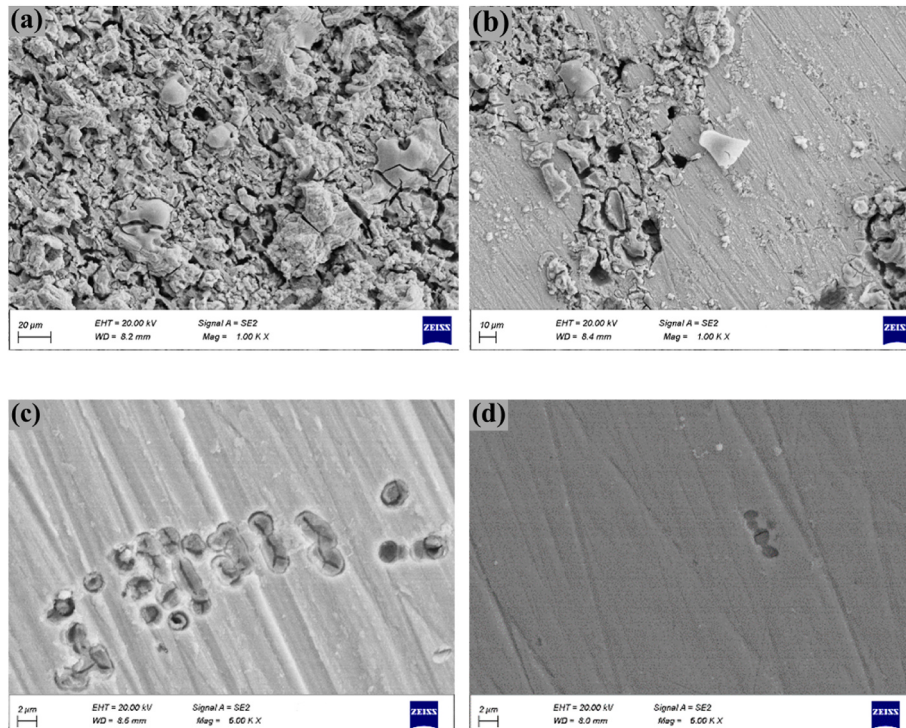


Fig. 7. SEM micrographs of the corroded surfaces of $\text{Cu}_{50}\text{Zr}_{43}\text{Al}_7$ in a) 1 M HCl and c) 0.6 M NaCl for 24 h, and $(\text{Cu}_{50}\text{Zr}_{43}\text{Al}_7)_{96}\text{Y}_4$ in b) 1 M HCl and d) 0.6 M NaCl for 24 h.

lower corrosion current density (i_{corr}) than copper. With the addition of 2% Y, corrosion current density decreased from $120.5 \mu\text{A}/\text{cm}^2$ to $53.8 \mu\text{A}/\text{cm}^2$. With a further increase of Y to 4%, the corrosion current density reached its lowest value among the samples tested. A similar trend was observed in 0.6 M NaCl solution and $(\text{Cu}_{50}\text{Zr}_{43}\text{Al}_7)_{96}\text{Y}_4$ sample shows the lowest corrosion current density of $1.5 \mu\text{A}/\text{cm}^2$.

The rationalization of the effect of Y on the corrosion of $\text{Cu}_{50}\text{Zr}_{43}\text{Al}_7$ can be ascertained from the potentiodynamic polarization testing results. There is an apparent decrease in the cathodic kinetics with composition. As measured upon pure Cu, the rate of cathodic kinetics is comparatively high, because Cu is particularly good with electron transfer reactions (i.e., the cathodic reaction of oxygen reduction). Consequently, pure Cu has a relatively high E_{OCP} (and E_{corr}) as a result of its rapid cathodic kinetics. The BMG specimens that contain 50 at % Cu, have notably lower rates of cathodic kinetics, resulting in both a lower E_{OCP} and E_{corr} for the BMG specimens. As Y (and rare-earth elements) are ineffective at electron transfer reactions, the cathodic kinetics of specimens containing Y, reveal a decrease in cathodic kinetics with increasing Y content (which incidentally, decreases Cu content simultaneously). In addition, although the effect on corrosion of which is not possible to isolate, Y has a strong atomic bond with other elements in the system because of its high negative mixing enthalpy [26]. From the results herein, it can be reported that Y serves as to decrease the corrosion rate of the BMG studied, by decreasing the rate of the cathodic partial

reaction.

To complement the electrochemical investigation, and to investigate the longer term and physical corrosion behavior, specimens were also immersed in a 1 M HCl and 0.6 M NaCl solution for 24 h. Following some hours of immersion in HCl, corrosion products on the surface were visible to the naked eye. In the case of $\text{Cu}_{50}\text{Zr}_{43}\text{Al}_7$, the sample after 24 h was completely covered by corrosion products. Fig. 7 (a) and (b) display the surface morphology of the samples after 24 h of immersion in HCl solution. As can be seen, increasing Y content reduces corrosion the prevalence of products on the surface, with some areas apparently without any obvious corrosion product. The EDS analysis of these products revealed the surface film/products to be principally composed of O, Cu and Zr. That means the resulting film is a mixture of simple and/or complex oxide compounds of the constituent elements of the sample. Similarly, Ke et al. [48] reported the presence of O, Zr, Ti and Cu in corrosion products at the surface of $\text{Cu}_{60}\text{Zr}_{30}\text{Ti}_{10}$ after immersion in HCl solutions of $>[0.5 \text{ M}]$.

Following a few hours in the 0.6 M NaCl, there was no significant evidence of corrosion or corrosion products upon the surface of test specimens. As shown in Fig. 7 (c) and 7 (d), only discrete pits were seen on the surface of specimens, with an increase in the Y content decreasing the number and the apparent depth of such sites of localised corrosion.

For the conditions explored in this study, the conditions revealed that none of the specimens tested could develop a passive layer (Fig. 6)

Table 3

Comparison between $(\text{Cu}_{50}\text{Zr}_{43}\text{Al}_7)_{100-x}\text{Y}_x$ BMGs and some other BMGs in i_{corr} (0.6 M NaCl), GFA, and σ_f values.

Alloy	i_{corr} ($\mu\text{A}/\text{cm}^2$)	GFA (mm)	σ_f (MPa)	Ref.
$\text{Cu}_{50}\text{Zr}_{43}\text{Al}_7$	4.4	10	2006	This work
$(\text{Cu}_{50}\text{Zr}_{43}\text{Al}_7)_{98}\text{Y}_2$	3.1	15	1920	This work
$(\text{Cu}_{50}\text{Zr}_{43}\text{Al}_7)_{96}\text{Y}_4$	1.5	12	1787	This work
$\text{Zr}_{46}\text{Cu}_{46}\text{Al}_8$	0.59	4.2	1900	[54,55]
$\text{Zr}_{50}\text{Cu}_{40}\text{Al}_{10}$	0.75	8	1859	[56,57]
$\text{Cu}_{50}\text{Zr}_{30}\text{Ti}_{10}$	4.3	2	2090	[58,59]
$\text{Zr}_{55}\text{Ti}_3\text{Cu}_{32}\text{Al}_{10}$	0.042	4	1695	[60]
$\text{Zr}_{55}\text{Ti}_3\text{Hf}_1\text{Cu}_{31}\text{Al}_{10}$	0.04	4	1716	[60]
$\text{Zr}_{55}\text{Ti}_3\text{Hf}_3\text{Cu}_{29}\text{Al}_{10}$	0.038	8	1800	[60]
$\text{Zr}_{55}\text{Ti}_3\text{Hf}_5\text{Cu}_{27}\text{Al}_{10}$	0.037	6	1780	[60]
$\text{Zr}_{60}\text{Fe}_{10}\text{Cu}_{20}\text{Al}_{10}$	9.71	10	1708	[61,62]
$\text{Zr}_{65}\text{Cu}_{17.5}\text{Fe}_{10}\text{Al}_{7.5}$	0.172	2	1745	[63]
$\text{Ti}_{25}\text{Zr}_{25}\text{Cu}_{25}\text{Ni}_{25}$	20.719	–	1616	[64]
$\text{Ti}_{30}\text{Zr}_{30}\text{Cu}_{20}\text{Ni}_{20}$	20.173	–	1837	[64]
$\text{Ti}_{35}\text{Zr}_{35}\text{Cu}_{15}\text{Ni}_{15}$	11.139	–	2034	[64]
$\text{Ti}_{40}\text{Zr}_{40}\text{Cu}_{10}\text{Ni}_{10}$	10128	–	2204	[64]

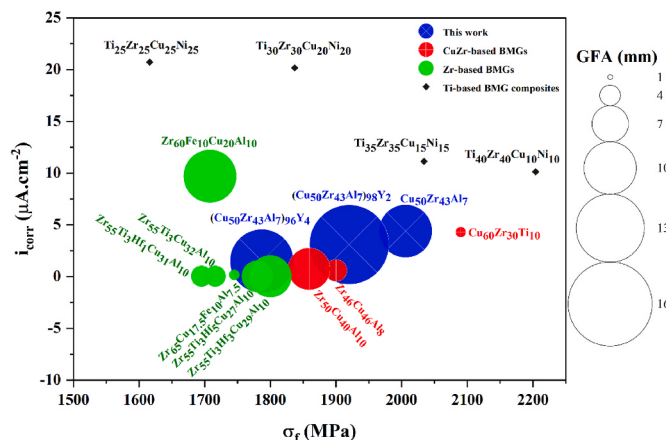


Fig. 8. Comparison between $(\text{Cu}_{50}\text{Zr}_{43}\text{Al}_7)_{100-x}\text{Y}_x$ BMGs and literature reported BMGs for i_{corr} (0.6 M NaCl), GFA, and σ_f values.

and specimens were prone to pitting corrosion in either 0.6 M NaCl or 1 M HCl. In the presence of such chloride containing solutions, the corrosion mechanism of metallic glasses was pitting corrosion. It would appear that the E_{corr} of the specimens in the conditions tested is above the E_{pit} (pitting potential) of the specimens, and corrosion rates are appreciable. Ideally metallic glasses may be physically and chemically homogeneous and free of secondary phases or defects. Nonetheless, the presence of these heterogeneities in as-cast samples is unavoidable. Therefore, the presence of structural heterogeneities may contribute to the formation of such localized corrosion [49–52]. Zander et al. [53] reported Cu-Zr-Al-Y bulk metallic glass shows good corrosion resistance in NaCl with a low molarity of 0.001 M due to the formation of protective oxide films. However, the passive layer did not form at higher NaCl molarity (0.01 M) and hence the alloy was susceptible to pitting corrosion.

In summation, the developed alloys in this work revealed a promising combination of mechanical properties, glass forming ability and corrosion rate. In order to have a clear picture of the interplay between the, i_{corr} , GFA, and σ_f values of BMGs from the current study were compared with some other BMGs reported in literature (Table 3). It may be observed from Fig. 8, that $(\text{Cu}_{50}\text{Zr}_{43}\text{Al}_7)_{100-x}\text{Y}_x$ BMGs, and especially $(\text{Cu}_{50}\text{Zr}_{43}\text{Al}_7)_{98}\text{Y}_2$, shows a unique combination of high GFA, high strength and appropriate corrosion rate. The Cu based BMGs studied herein do not have as low a corrosion rate as Zr rich BMGs, however, have a significantly lower cost, and higher GFA and strength. In addition, $(\text{Cu}_{50}\text{Zr}_{43}\text{Al}_7)_{100-x}\text{Y}_x$ BMGs exhibited much higher GFAs, a lower

corrosion rate, and approximately the same strength as Ti-based BMG composites (amorphous-crystalline phases). This places the Cu-based BMGs reported herein in unique property space, as a promising BMG system.

4. Conclusions

In this study, the effects of Y additions to the $\text{Cu}_{50}\text{Zr}_{43}\text{Al}_7$ BMG were studied with the aim of obtaining a combination of high GFA, mechanical properties, and corrosion resistance. The results herein indicated that the addition of Y can improve the GFA, and a fully amorphous rod with diameter of 15 mm was achieved for the $(\text{Cu}_{50}\text{Zr}_{43}\text{Al}_7)_{98}\text{Y}_2$ alloy. The mechanical properties of as-cast $(\text{Cu}_{50}\text{Zr}_{43}\text{Al}_7)_{100-x}\text{Y}_x$ ($x = 0, 2$ and 4 at. %) BMGs were examined by compressive testing at room temperature. The fully bulk amorphous Cu-based alloys exhibit good mechanical properties, i.e., the compressive fracture strength (σ_{cf}) of 1787–2006 MPa with Young's modulus of higher than 100 GPa.

Electrochemical impedance spectroscopy and potentiodynamic polarization experiments revealed that the Y addition to $\text{Cu}_{50}\text{Zr}_{43}\text{Al}_7$ BMG decreased the corrosion rate, and the $(\text{Cu}_{50}\text{Zr}_{43}\text{Al}_7)_{96}\text{Y}_4$ BMG revealed the lowest corrosion rate in both 0.6 M NaCl and 1 M HCl. The role of Y in decreasing the cathodic reaction kinetics upon the $\text{Cu}_{50}\text{Zr}_{43}\text{Al}_7$ BMG was ascribed for the controlling the kinetics of the corrosion rate for the BMGs studied. The combination of strength, excellent glass forming ability and (moderate) corrosion rate of Y-containing Cu-Zr-Al BMG makes this alloy system promising alloy system.

CRediT authorship contribution statement

Mehdi Malekan: Conceptualization, Methodology, Formal analysis, Writing - Review & Editing, Supervision, Project administration, Funding acquisition.

Reza Rashidi: Methodology, Formal analysis, Investigation, Writing - original draft.

Mansoor Bozorg: Methodology, Formal analysis, Investigation, Writing - Review & Editing.

Nick Birbilis: Conceptualization, Methodology, Formal analysis, Writing - Review & Editing, Supervision.

Declaration of competing interest

The authors declare that they have no known competing financial interests or personal relationships that could have appeared to influence the work reported in this paper.

Data availability

No data was used for the research described in the article.

Acknowledgments

Financial support by the University of Tehran is gratefully acknowledged.

References

- [1] A. Inoue, Stabilization of metallic supercooled liquid and bulk amorphous alloys, *Acta Mater.* 48 (1) (2000) 279–306.
- [2] C.A. Schuh, T.C. Hufnagel, U. Ramamurty, Mechanical behavior of amorphous alloys, *Acta Mater.* 55 (12) (2007) 4067–4109.
- [3] K. Asami, C.-L. Qin, T. Zhang, A. Inoue, Effect of additional elements on the corrosion behavior of a Cu-Zr-Ti bulk metallic glass, *Mater. Sci. Eng., A* 375 (2004) 235–239.
- [4] A. Inoue, A. Takeuchi, Recent development and application products of bulk glassy alloys, *Acta Mater.* 59 (6) (2011) 2243–2267.
- [5] J. Gu, M. Song, S. Ni, X. Liao, S. Guo, Improving the plasticity of bulk metallic glasses via pre-compression below the yield stress, *Mater. Sci. Eng., A* 602 (2014) 68–76.

- [6] A. Inoue, W. Zhang, T. Zhang, K. Kurosaka, High-strength Cu-based bulk glassy alloys in Cu–Zr–Ti and Cu–Hf–Ti ternary systems, *Acta Mater.* 49 (14) (2001) 2645–2652.
- [7] T. Zhang, H. Men, S. Pang, J. Fu, C. Ma, A. Inoue, Effects of a minor addition of Si and/or Sn on formation and mechanical properties of Cu–Zr–Ti bulk metallic glass, *Mater. Sci. Eng., A* 449 (2007) 295–298.
- [8] M. Malekan, S. Shabestari, R. Gholamipour, S. Seyedehin, Effect of Ge addition on mechanical properties and fracture behavior of Cu–Zr–Al bulk metallic glass, *J. Alloys Compd.* 484 (1–2) (2009) 708–711.
- [9] M. Malekan, S. Shabestari, W. Zhang, S. Seyedehin, R. Gholamipour, A. Makino, A. Inoue, Effect of Si addition on glass-forming ability and mechanical properties of Cu–Zr–Al bulk metallic glass, *Mater. Sci. Eng., A* 527 (27–28) (2010) 7192–7196.
- [10] L. Deng, B. Zhou, H. Yang, X. Jiang, B. Jiang, X. Zhang, Roles of minor rare-earth elements addition in formation and properties of Cu–Zr–Al bulk metallic glasses, *J. Alloys Compd.* 632 (2015) 429–434.
- [11] R. Rashidi, M. Malekan, R. Gholamipour, Microstructure and mechanical properties of a Cu–Zr based bulk metallic glass containing atomic scale chemical heterogeneities, *Mater. Sci. Eng., A* 729 (2018) 433–438.
- [12] M. Malekan, R. Rashidi, S.G. Shabestari, Mechanical properties and crystallization kinetics of Er-containing Cu–Zr–Al bulk metallic glasses with excellent glass forming ability, *Vacuum* 174 (2020), 109223.
- [13] M. Malekan, R. Rashidi, Effective role of minor silicon addition on crystallization kinetics of Cu₅₀Zr₄₃Al₇ bulk metallic glass, *Appl. Phys. A* 127 (4) (2021) 246.
- [14] A. Jalali, M. Malekan, E.S. Park, R. Rashidi, A. Bahmani, G.H. Yoo, Deformation behavior of Zr₃₃Hf₈Ti₆Cu₃₂Ni₁₀Co₅Al₆ high-entropy bulk metallic glass and Cu₄₇Zr₄₇Al₆ low-entropy bulk metallic glass at room and high temperatures, *Mater. Sci. Eng., A* 832 (2022), 142499.
- [15] C. Suryanarayana, A. Inoue, *Bulk Metallic Glasses*, CRC press, 2017.
- [16] H.-w. Xu, Y.-l. Du, D. Yu, Effects of Y addition on structural and mechanical properties of Cu₂ZrAl bulk metallic glass, *Trans. Nonferrous Metals Soc. China* 22 (4) (2012) 842–846.
- [17] Y. Zhang, J. Chen, G. Chen, X. Liu, Influence of yttrium addition on the glass forming ability in Cu–Zr–Al alloys, *Mater. Sci. Eng., A* 483 (2008) 235–238.
- [18] T. Zhang, K. Kurosaka, A. Inoue, Thermal and mechanical properties of Cu-based Cu–Zr–Ti–Y bulk glassy alloys, *Mater. Trans.* 42 (10) (2001) 2042–2045.
- [19] B. Li, J. Li, X. Fan, J. Chen, Formation of bulk metallic glasses from Cu–Zr based alloys with yttrium addition, *Rare Met. Mater. Eng.* 43 (7) (2014) 1558–1561.
- [20] D. Xu, G. Duan, W.L. Johnson, Unusual glass-forming ability of bulk amorphous alloys based on ordinary metal copper, *Phys. Rev. Lett.* 92 (24) (2004), 245504.
- [21] X.P. Nie, X.H. Yang, J.Z. Jiang, Ti microalloying effect on corrosion resistance and thermal stability of Cu₂Zr-based bulk metallic glasses, *J. Alloys Compd.* 481 (1–2) (2009) 498–502.
- [22] M.K. Tam, S.J. Pang, C.H. Shek, Corrosion behavior and glass-forming ability of Cu–Zr–Al–Nb alloys, *J. Non-Cryst. Solids* 353 (32–40) (2007) 3596–3599.
- [23] C. Zhang, N. Qiu, L. Kong, X. Yang, H. Li, Thermodynamic and structural basis for electrochemical response of Cu–Zr based metallic glass, *J. Alloys Compd.* 645 (2015) 487–490.
- [24] N. Hua, L. Huang, J. Wang, Y. Cao, W. He, S. Pang, T. Zhang, Corrosion behavior and in vitro biocompatibility of Zr–Al–Co–Ag bulk metallic glasses: an experimental case study, *J. Non-Cryst. Solids* 358 (12) (2012) 1599–1604.
- [25] P. Jinhong, P. Ye, W. Jili, H. Xiancong, Influence of minor addition of in on corrosion resistance of Cu-based bulk metallic glasses in 3.5% NaCl solution, *Rare Met. Mater. Eng.* 43 (1) (2014) 32–35.
- [26] M. Malekan, R. Rashidi, S.G. Shabestari, J. Eckert, Thermodynamic and kinetic interpretation of the glass-forming ability of Y-containing Cu–Zr–Al bulk metallic glasses, *J. Non-Cryst. Solids* 576 (2022), 121266.
- [27] Y.Q. Cheng, E. Ma, H.W. Sheng, Atomic level structure in multicomponent bulk metallic glass, *Phys. Rev. Lett.* 102 (2009), 245501.
- [28] Y.Q. Cheng, E. Ma, Atomic-level structure and structure–property relationship in metallic glasses, *Prog. Mater. Sci.* 56 (4) (2011) 379–473.
- [29] Y. Xu, Y. Wang, X. Liu, G. Chen, Y. Zhang, Effects of additional elements (M) on the thermal stability and structure of (Zr₅₂.2Cu₃₉.1Al₈)₇100–xMx (M = Ag, Be, Cd, x = 8, 7, 2) amorphous alloys, *J. Mater. Sci.* 44 (2009) 3861–3866.
- [30] P. Yu, H.Y. Bai, W.H. Wang, Superior glass-forming ability of Cu₂Zr alloys from minor additions, *J. Mater. Res.* 21 (2006) 1674–1679.
- [31] Q. Wang, C.T. Liu, Y. Yang, J.B. Liu, Y.D. Dong, J. Lu, The atomic-scale mechanism for the enhanced glass-forming-ability of a Cu–Zr based bulk metallic glass with minor element additions, *Sci. Rep.* 4 (2014) 4648.
- [32] M. Lee, C.M. Lee, K.R. Lee, E. Ma, J.C. Lee, Networked interpenetrating connections of icosahedra: effects on shear transformations in metallic glass, *Acta Mater.* 59 (1) (2011) 159–170.
- [33] Ž.Z. Tasić, M.B. Petrović Mihajlović, M.B. Radovanović, A.T. Simonović, M. M. Antonijević, Cephradine as corrosion inhibitor for copper in 0.9% NaCl solution, *J. Mol. Struct.* 1159 (2018) 46–54.
- [34] Y. Qiang, S. Zhang, S. Yan, X. Zou, S. Chen, Three indazole derivatives as corrosion inhibitors of copper in a neutral chloride solution, *Corrosion Sci.* 126 (2017) 295–304.
- [35] S. Hong, W. Chen, H.Q. Luo, N.B. Li, Inhibition effect of 4-amino-antipyrine on the corrosion of copper in 3wt.% NaCl solution, *Corrosion Sci.* 57 (2012) 270–278.
- [36] D.-Q. Zhang, B. Xie, L.-X. Gao, Q.-R. Cai, H.G. Joo, K.Y. Lee, Intramolecular synergistic effect of glutamic acid, cysteine and glycine against copper corrosion in hydrochloric acid solution, *Thin Solid Films* 520 (1) (2011) 356–361.
- [37] A. Singh, Y. Lin, K.R. Ansari, M.A. Quraishi, E.E. Eboso, S. Chen, W. Liu, Electrochemical and surface studies of some Porphines as corrosion inhibitor for J55 steel in sweet corrosion environment, *Appl. Surf. Sci.* 359 (2015) 331–339.
- [38] B. Ngouné, M. Pengou, A.M. Nouteza, C.P. Nanseu-Njiki, E. Ngameni, Performances of alkaloid extract from *Rauvolfia macrophylla* Stapf toward corrosion inhibition of C38 steel in acidic media, *ACS Omega* 4 (5) (2019) 9081–9091.
- [39] E.A. Noor, Evaluation of inhibitive action of some quaternary N-heterocyclic compounds on the corrosion of Al–Cu alloy in hydrochloric acid, *Mater. Chem. Phys.* 114 (2) (2009) 533–541.
- [40] Z. Salarvand, M. Amirmasr, M. Talebian, K. Raeissi, S. Meghdadi, Enhanced corrosion resistance of mild steel in 1M HCl solution by trace amount of 2-phenylbenzothiazole derivatives: experimental, quantum chemical calculations and molecular dynamics (MD) simulation studies, *Corrosion Sci.* 114 (2017) 133–145.
- [41] Q. Deng, N.-N. Ding, X.-L. Wei, L. Cai, X.-P. He, Y.-T. Long, G.-R. Chen, K. Chen, Identification of diverse 1,2,3-triazole-connected benzyl glycoside-serine/threonine conjugates as potent corrosion inhibitors for mild steel in HCl, *Corrosion Sci.* 64 (2012) 64–73.
- [42] M.A. Amin, S.S. Abd El-Rehim, E.E.F. El-Sherbini, R.S. Bayoumi, The inhibition of low carbon steel corrosion in hydrochloric acid solutions by succinic acid: Part I. Weight loss, polarization, EIS, PZC, EDX and SEM studies, *Electrochim. Acta* 52 (11) (2007) 3588–3600.
- [43] M. Kissi, M. Boulkah, B. Hammouti, M. Benkaddour, Establishment of equivalent circuits from electrochemical impedance spectroscopy study of corrosion inhibition of steel by pyrazine in sulphuric acidic solution, *Appl. Surf. Sci.* 252 (12) (2006) 4190–4197.
- [44] P. Gong, D. Wang, C. Zhang, Y. Wang, Z. Jamili-Shirvan, K. Yao, X. Wang, Corrosion behavior of Ti₃Zr₆Be₂Cu (Ni) high-entropy bulk metallic glasses in 3.5 wt.% NaCl, *npj Materials Degradation* 6 (1) (2022) 1–14.
- [45] E.L. Su, X.Q. Wu, D.C. Zhang, Y. Li, J.G. Lin, Effects of Si additions on the glass-forming ability and corrosion resistance of Cu₄₉Zr₄₅Al₆ bulk metallic glass, *Corrosion* 69 (11) (2013) 1088–1094.
- [46] M.K. Tam, S.J. Pang, C.H. Shek, Effects of niobium on thermal stability and corrosion behavior of glassy Cu–Zr–Al–Nb alloys, *J. Phys. Chem. Solid.* 67 (4) (2006) 762–766.
- [47] M.K. Tam, S.J. Pang, C.H. Shek, Corrosion behavior and glass-forming ability of Cu–Zr–Al–Nb alloys, *J. Non-Cryst. Solids* 353 (32) (2007) 3596–3599.
- [48] W.-K. An, A.-h. Cai, X. Xiong, Y. Liu, Y. Luo, T.-L. Li, X.-S. Li, Corrosion behavior of Cu 60 Zr 30 Ti 10 metallic glass in the Cl⁻-containing solution, *Mater. Sci. Appl.* 2 (6) (2011) 546–554.
- [49] A. Gebert, U. Kuehn, S. Baunack, N. Mattern, L. Schultz, Pitting corrosion of zirconium-based bulk glass-matrix composites, *Mater. Sci. Eng., A* 415 (1) (2006) 242–249.
- [50] P.F. Gostin, A. Gebert, L. Schultz, Comparison of the corrosion of bulk amorphous steel with conventional steel, *Corrosion Sci.* 52 (1) (2010) 273–281.
- [51] Y. Zhu, W. Wang, Y. Song, S. Zhang, H. Li, A. Wang, H. Zhang, Z. Zhu, Atomic-scale Nb heterogeneity induced icosahedral short-range ordering in metallic glasses, *J. Mater. Sci. Technol.* 108 (2022) 73–81.
- [52] Y. Zhu, Y. Zhou, A. Wang, H. Li, H. Fu, H. Zhang, H. Zhang, Z. Zhu, Atomic-scale icosahedral short-range ordering in a rejuvenated Zr-based bulk metallic glass upon deep cryogenic treatment, *Mater. Sci. Eng., A* 850 (2022), 143565.
- [53] D. Zander, B. Heisterkamp, I. Gallino, Corrosion resistance of Cu–Zr–Al–Y and Cu–Zr–Ni–Al–Nb bulk metallic glasses, *J. Alloys Compd.* 434–435 (2007) 234–236.
- [54] W. Zhou, W.P. Weng, J.X. Hou, Glass-forming ability and corrosion resistance of ZrCuAlCo bulk metallic glass, *J. Mater. Sci. Technol.* 32 (4) (2016) 349–354.
- [55] W. Song, X. Meng, Y. Wu, D. Cao, H. Wang, X. Liu, X. Wang, Z. Lu, Improving plasticity of the Zr₄₆Cu₄₆Al₈ bulk metallic glass via thermal rejuvenation, *Sci. Bull.* 63 (13) (2018) 840–844.
- [56] B.A. Green, R.V. Steward, I. Kim, C.K. Choi, P.K. Liaw, K.D. Kihm, Y. Yokoyama, In situ observation of pitting corrosion of the Zr₅₀Cu₄₀Al₁₀ bulk metallic glass, *Intermetallics* 17 (7) (2009) 568–571.
- [57] G.Y. Wang, P.K. Liaw, Y. Yokoyama, M. Freels, R.A. Buchanan, A. Inoue, C. R. Brooks, Effects of partial crystallization on compression and fatigue behavior of Zr-based bulk metallic glasses, *J. Mater. Res.* 22 (2) (2007) 493–500.
- [58] P.-Y. Lee, Y.-M. Cheng, J.-Y. Chen, C.-J. Hu, Formation and corrosion behavior of mechanically-alloyed Cu–Zr–Ti bulk metallic glasses, *Metals* 7 (4) (2017) 148.
- [59] E.S. Park, H.J. Chang, D.H. Kim, T. Ohkubo, K. Hono, Effect of the substitution of Ag and Ni for Cu on the glass forming ability and plasticity of Cu₆₀Zr₃₀Ti₁₀ alloy, *Scripta Mater.* 54 (9) (2006) 1569–1573.
- [60] Z.S. Jin, Y.J. Yang, Z.P. Zhang, X.Z. Ma, J.W. Lv, F.L. Wang, M.Z. Ma, X.Y. Zhang, R.P. Liu, Effect of Hf substitution Cu on glass-forming ability, mechanical properties and corrosion resistance of Ni-free Zr–Ti–Cu–Al bulk metallic glasses, *J. Alloys Compd.* 806 (2019) 668–675.
- [61] Y. Luo, Y. Jiang, P. Zhang, X. Wang, H. Ke, P. Zhang, A novel Ni-free Zr-based bulk metallic glass with high glass forming ability, corrosion resistance and thermal stability, *Chin. J. Mech. Eng.* 33 (1) (2020) 65.
- [62] Q.S. Zhang, W. Zhang, D.V. Louguine-Luzgin, A. Inoue, High glass-forming ability and unusual deformation behavior of new Zr–Cu–Fe–Al bulk metallic glasses, *Mater. Sci. Forum* 654–656 (2010) 1042–1045.
- [63] M. Zhou, K. Hagos, H. Huang, M. Yang, L. Ma, Improved mechanical properties and pitting corrosion resistance of Zr₆₅Cu_{17.5}Fe₁₀Al_{7.5} bulk metallic glass by isothermal annealing, *J. Non-Cryst. Solids* 452 (2016) 50–56.
- [64] Q. Li, S.S. Liu, X.H. Wang, T. Yang, C. Dong, J.T. Hu, Y.Q. Jiang, Mechanical and corrosion properties of Ti–Ni–Cu–Zr metallic glass matrix composites, *J. Alloys Compd.* 727 (2017) 1344–1350.